

## INTERCALATE LAYER STRUCTURE IN GRAPHITE-ALKALI METAL COMPOUNDS

M. S. DRESSELHAUS\*, N. KAMBE\*, A. N. BERKER\*\* and G. DRESSELHAUS\*\*\*  
*Massachusetts Institute of Technology, Cambridge, MA 02139 (U.S.A.)*

(Received June 16, 1980)

### Summary

Electron diffraction and real space imaging provide important tools for the study of in-plane structure of graphite intercalation compounds because of the small size of the electron beam in an electron microscope. Good agreement is obtained between measurements made by electron diffraction and other techniques for the transition temperatures  $T_1$  and  $T_u$  for stage 2 graphite-K and graphite-Rb compounds and for the  $\vec{q}$  vectors for the prominent diffraction peaks in the various temperature regimes. Analysis of the real space images and the electron diffraction patterns provide strong evidence for the coexistence of multiple phases in these stage 2 compounds. The use of X-ray intensity measurements to yield information on the in-plane density and the intercalate layer stacking order is indicated.

The principal method for the determination of the intercalate layer structure is analysis of ( $hkl$ ) diffraction peak positions and intensities. In many cases the number of atoms per unit cell is large, and the symmetry is low, so that a larger number of ( $hkl$ ) reflections is required for a definitive analysis than is available experimentally. The analysis of diffraction data is further complicated by the presence of stacking faults among the graphite layers and coexisting phases within the dimensions of the incident X-ray, electron or neutron beams. Nevertheless, it is possible to obtain important information about the in-plane structure of the intercalant even though the materials lack sufficient perfection to allow a complete crystallographic structural analysis. In this paper ( $hk0$ ) electron diffraction measurements together with several physical arguments are brought to bear on the intercalant ordering, and a number of important conclusions are reached with

\*Department of Electrical Engineering and Computer Science and Center for Materials Science and Engineering.

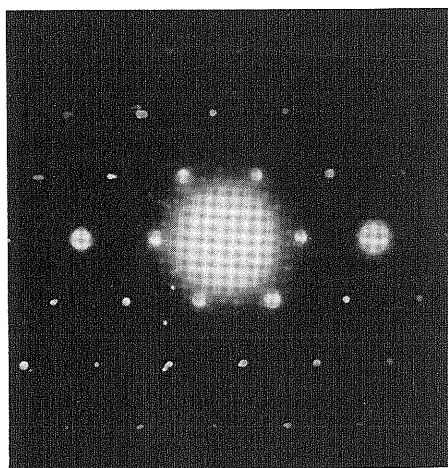
\*\*Department of Physics and Center for Materials Science and Engineering.

\*\*\*Francis Bitter National Magnet Laboratory, supported by NSF.

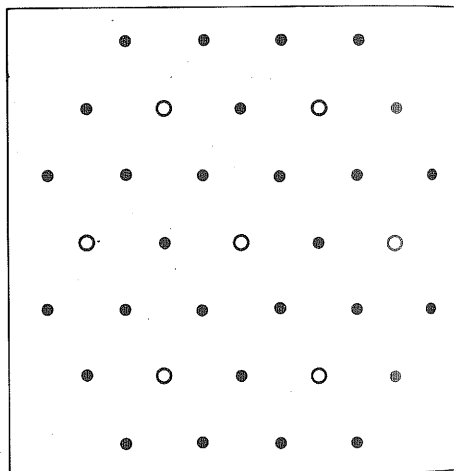
regard to coexisting phases, in-plane densities and interlayer intercalate correlation.

Because the illuminated specimen area by an electron beam (e.g., from a Philips EM 300 electron microscope operating at 100 keV) is typically  $\leq 1 \mu\text{m}$ , it is possible to probe graphite intercalation compounds based on highly oriented pyrolytic graphite (HOPG) within a single crystallite of the host material. By study of the superlattice patterns of  $(hk0)$  reflections obtained by electron diffraction of an electron beam through a thin sample ( $\leq 1000 \text{ \AA}$ ), detailed information about the basic in-plane ordering can be obtained. In simple cases, the superlattice can be identified directly from the diffraction patterns, as, for example, for the  $p(2 \times 2)R0^\circ$  and the  $p(\sqrt{3} \times \sqrt{3})R30^\circ$  superlattices which are found for  $\text{C}_8\text{Rb}$  (stage 1) and  $\text{C}_6\text{Li}$  (stage 1), respectively. A diffraction pattern corresponding to a  $p(2 \times 2)$  superlattice for  $\text{C}_8\text{Rb}$  at room temperature is shown in Fig. 1.

Definitive information on the interlayer intercalate stacking order is also provided from  $(hk0)$  reflections in the special cases where the intercalant on adjacent layers follows sequential occupation of *all* equivalent lattice sites, as, for example, the  $\alpha\beta\gamma\delta$  sites of the  $p(2 \times 2)$  structure or the  $\alpha\beta\gamma$  sites of the  $p(\sqrt{3} \times \sqrt{3})$  structure shown in Fig. 2. For such sequential intercalate stacking over  $\alpha_m$  equivalent intercalate sites, the structure factor  $F_{hk0}$  vanishes, and the superlattice disappears, leaving only the  $p(1 \times 1)$  graphite spot pattern which is contained in all electron diffraction patterns that have been reported for graphite intercalation compounds [1 - 3]. The vanishing structure factor is found by summation over the sequentially occupied intercalate sites  $\alpha_1 \dots \alpha_m$ ,



(a)



(b)

Fig. 1. (a) In-plane electron diffraction pattern for a  $\text{C}_8\text{Rb}$  stage 1 sample for  $T \geq 300 \text{ K}$ . (b) A schematic representation of the diffraction pattern of (a) consistent with a  $p(2 \times 2)R0^\circ$  superlattice.



(a)

Fig. 2. Real space diagram showing the arrangement of carbon atoms (represented by circles) and intercalate sites (represented by dots) in a graphite lattice. The diagram illustrates the  $p(2 \times 2)$  superlattice structure.

$$F_{hk0} =$$

where the  $\alpha_m$  layers of intercalate are sequentially occupied and occurs. The vanishing of the structure factor is found by summation over the sequentially occupied intercalate sites  $\alpha_1 \dots \alpha_m$ .

Although the structure factor  $F_{hk0}$  normally vanishes for sequential occupation, it is possible to consider the possibility of a non-vanishing structure factor if the intercalate sites are not sequentially occupied. This idea of a non-vanishing structure factor for low stage intercalation compounds has been proposed by [1 - 3].

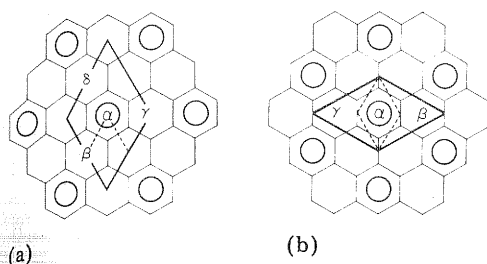


Fig. 2. Real space in-plane projection of superlattice structures. The circles denote the intercalate atoms (ions) which are superimposed on the graphite hexagonal network where carbon atoms are located at the corner sites. The in-plane unit cells for the superlattice are indicated by heavy lines and the dashed lines denote the corresponding unit cell for graphite. (a) The  $p(2 \times 2)R0^\circ$  superlattice. The intercalate is shown for a layer where the  $\alpha$  sites are occupied. The  $\beta$ ,  $\gamma$ ,  $\delta$  sites are crystallographically equivalent. (b) The  $p(\sqrt{3} \times \sqrt{3})R30^\circ$  superlattice where the intercalate is shown on a layer where the  $\alpha$  sites are occupied. The  $\beta$  and  $\gamma$  sites are crystallographically equivalent.

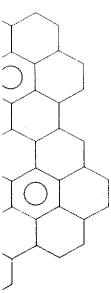
$$F_{hk0} = \sum_{j=\alpha_1}^{\alpha_m} f \exp\{-2\pi i(hu_j + kv_j)\} = 0 \quad (1)$$

where the  $u_j$ ,  $v_j$  are the in-plane ( $x, y$ ) intercalate coordinates on each of the  $\alpha_m$  layers of the unit cell, and  $f$  is the atomic scattering factor. It must be emphasized that the vanishing of the  $F_{hk0}$  structure factor is very restrictive and occurs only under very special circumstances such as the ordered sequential occupation of all  $\alpha_m$  sites in the stacking sequence. Thus, the disappearance of the  $p(2 \times 2)R0^\circ$  superlattice for  $C_8Rb$  below  $\sim 300$  K [2], and of the  $p(\sqrt{3} \times \sqrt{3})R30^\circ$  superlattice for  $C_6Li$  below  $\sim 220$  K [1], provides compelling evidence for  $\alpha\beta\gamma\delta$  and  $\alpha\beta\gamma$  intercalate interlayer stacking in these samples below the indicated transition temperatures.

Although this high degree of intercalate interlayer stacking order is not normally found in graphite intercalation compounds, intercalate interlayer correlation is expected to occur in low stage compounds. In this connection, consider the  $n$  carbon layers of a stage  $n$  compound to form a slightly deformable sheet as shown in Fig. 3. Since intercalate atoms or molecules tend to be large compared with carbon atoms, the intercalant introduces a local strain in the vicinity of each intercalate site, perhaps giving rise to a puckering of the carbon atoms or a deformation of the graphite layers in the vicinity of the intercalant. Whether the intercalate interlayer interaction is due to an elastic or electrostatic mechanism, the interaction is repulsive. Thus, if an intercalate atom is in position  $\alpha$  on one layer, the strain on the deformable sheet is lowered by *not* placing the intercalant on the next layer on an  $\alpha$  site. This idea of intercalate interlayer exclusion, fully compatible with the highly ordered  $\alpha\beta\gamma\delta$  and  $\alpha\beta\gamma$  stacking arrangements discussed above for first stage  $C_8Rb$  and  $C_6Li$ , also gives rise to a short-range intercalate interlayer correlation for low stage compounds that have either commensurate or incommensurate intercalate ordering with respect to the graphite bounding layer. For

ple for  $T \geq 300$  K.  
it with a  $p(2 \times 2)R0^\circ$





For the various in-plane structures that are observed for the alkali metal compounds for stages  $n \geq 2$  there appears to be a strong correlation between the in-plane areas of a unit cell in the intercalant layer  $A_i$  with an area  $A_m$  in the parent metal, defined by  $V_m/(\sqrt{3}a_x^0/2)$ , where  $V_m$  is the volume of the metallic unit cell,  $\sqrt{3}a_x^0/2$  is the nearest-neighbor metal distance, and  $a_x^0$  is the metallic lattice constant [9]. This close correlation between  $A_i$  and  $A_m$  is shown in Table 1. It is also of interest to note that although the  $h(\sqrt{12} \times \sqrt{12})R30^\circ$  structure has not been obtained from direct analysis of diffraction patterns for the potassium compounds, the intercalant area  $A_i$  is  $15.72 \text{ (\AA)}^2$  for the  $h(\sqrt{12} \times \sqrt{12})R30^\circ$  structure, in excellent agreement with  $A_m = 15.79 \text{ (\AA)}^2$  for metallic potassium. Since the  $h(\sqrt{12} \times \sqrt{12})R30^\circ$  structure is not present, then two (of many) possibilities for the intercalant configuration are a triangular lattice with a lattice constant  $\sqrt{6}a_0$  or the coexistence of two primitive superlattice phases (such as the  $\sqrt{3} \times \sqrt{3}$  and  $\sqrt{7} \times \sqrt{7}$ ) with relative concentrations yielding the proper in-plane density.

The value for the in-plane intercalate density is a matter of interest and importance. If the samples were completely stoichiometric and no vacancies (or interstitials) occurred in the intercalate layers, then the in-plane intercalate densities are directly given by the ideal chemical formula. From the metallic area  $A_m$ , a metallic in-plane density  $(1/\xi)_m$  for each of the intercalants of Table 1 can be determined, and these results are also included in the Table, showing that for Li, Na and K,  $\xi_m$  is approximately 6, 8 and 12, respectively. It is further noted that  $\xi_m$  increases beyond 12 for the heavier alkali metals with larger metallic radii. Finally, the in-plane intercalate densities  $(1/\xi)$  can be determined experimentally from  $(00l)$  intensity measurements [10]. Presently available experimental results for  $\xi$  are given in Table 1, showing generally good agreement with  $\xi_m$ , but significant departures from the commonly quoted stoichiometric values of  $\xi = 12$  for the intercalants, K, Rb and Cs.

An X-ray structure determination for an ordered crystal makes use of both  $(hkl)$  peak positions and integrated intensities in the diffraction pattern, yielding the space group, atom positions, vacancy concentration, temperature-dependent mean square atomic displacements by well-established computer minimization procedures. The application of these techniques to graphite intercalation compounds has been pioneered by groups led by Parry and Hérold [11, 12]. The work of Leung *et al.* [10] has focussed on the use of  $(00l)$  integrated intensity data to determine in-plane intercalate densities and temperature-dependent mean square  $c$ -axis displacements.

Integrated intensity measurements for  $(hkl)$  reflections can also be used to provide information on the interlayer stacking of the intercalant and of the graphite layers. This is illustrated in Table 2 where calculated intensities are given for several  $(hkl)$  reflections for stage 3 graphite-potassium with an in-plane  $p(2 \times 2)$  superlattice structure for several possible intercalant stacking sequences ( $\alpha\alpha$ ,  $\alpha\beta$ ,  $\alpha\beta\gamma$ ,  $\alpha\beta\gamma\delta$ ). The intensities in this Table have been calculated for the graphite layer stacking sequences (ABAXABAX). A  $p(2 \times 2)$  superlattice structure has recently been reported for stage 3 graphite-potas-

on. If the inter-  
intercalant most

$\sqrt{19.1^\circ}$  superlattice,  
the superlattice is  
the 7 equivalent

n Fig. 4, which  
kali metal com-  
l with the full  
 $\alpha_7$ , though short-  
e is likely to  
te exclusion  
ing in first stage  
also evidence for  
etal compounds  
pointed out that  
white-Li com-  
on and electro-  
mical bonding  
ase.

have exhibited  
ated by close-  
e of the unit cell,  
superlattices are  
 $\sqrt{19.1^\circ}$ ,  $p(3 \times 3)$   
action studies on  
entification has  
n-primitive struc-  
 $\sqrt{12}R30^\circ$   
only reported for

TABLE 1

Metallic in-plane areas in relation to areas of unit cells for higher stage alkali metal compounds (stage  $n \geq 2$ )

B.C.C. metal	$a_X^*$ (Å)	$V_m^3$ (Å) <sup>3</sup>	Metallic area $A_m^{**}$ in (Å) <sup>2</sup>	Dominant in-plane structure ( $n \geq 2$ )	Intercalant in-plane area $A_i^{***}$ in (Å) <sup>2</sup>	Calculated $\xi$ from metallic area $A_m^\dagger$ in $C_\xi X$	Measured $\xi$ from (001) intensities <sup>††</sup>
Li	3.51	21.62	7.11	$p(\sqrt{3} \times \sqrt{3})R30^\circ$	$\frac{3\sqrt{3}}{4} a_0^2 = 7.86$	5.43	—
Na	4.29	39.48	10.61	$p(2 \times 2)R0^\circ$	$3a_0^2 = 10.48$	8.10	—
K	5.23	71.53	15.79	mixed	—	12.05	10.5
Rb	5.59	87.34	18.05	$p(\sqrt{7} \times \sqrt{7})R19.1^\circ$	$\frac{7}{4} \sqrt{3} a_0^2 = 18.34$	13.88	14.0
Cs	6.05	110.72	21.13	incommensurate	—	16.13	16.4

\*B.C.C. lattice constants  $a_X^*$  taken from Wyckoff (ref. 9).\*\*Metallic area  $A_m = V_m / \left( \frac{\sqrt{3}}{2} a_X^* \right) = (a_X^*)^2 / \sqrt{3}$ .\*\*\*The intercalant in-plane area  $A_i$  refers to the superlattice unit cell.†The calculated reciprocal in-plane density  $\xi$  in the chemical formula  $C_\xi X$  is found directly from the metallic area  $A_m$ .††Experimental values for  $\xi$  taken from ref. 10.

TABLE 2

Calculated X  
calate interla

(hkl)	
100	1
210	2
200	2
310	3

\*The intensi  
tains contribu  
\*\*System is n  
with the 3 possium above  
measuremen  
tensity meas  
possible stac

The dei  
for stages  $n \geq$   
geometric ar  
For example  
transitions, tl  
and are chara  
ment is obtai  
X-ray [6, 15  
transition ter  
(2)  $T_1 < T <$   
electron diffr  
lattice behavi  
incommensur  
tion patterns  
dicative of co  
coexisting ora  
the disorderec  
workers for  $T$   
Despite differ  
that there is si  
diffraction da

On the b.  
electron diffra  
regimes for sta  
pattern is cons  
stacking and a  
of  $p(\sqrt{7} \times \sqrt{7})$   
fraction patter

TABLE 2

Calculated X-ray intensities for stage 3 graphite-K assuming various intercalate interlayer stackings in a  $(2 \times 2)$  superlattice\*

$(hkl)$	$ q $ in $(\text{\AA}^{-1})$	$\alpha$	$\alpha\beta^{**}$	$\alpha\beta\gamma$	$\alpha\beta\gamma\delta$
100	1.477	0.553	0.184	0.061	0.0
210	2.558	0.389	0.130	0.043	0.0
200	2.954	1.000	1.000	1.000	1.000
310	3.908	0.242	0.081	0.027	0.0

\*The intensities are normalized to the (200) diffraction line which contains contributions from both the potassium and the graphite layers.

\*\*System is not hexagonal. We assume an equal distribution of domains with the 3 possible orientations.

sium above  $\sim 2$  kbar pressure on the basis of single crystal X-ray diffraction measurements [13]. The results of Table 2 provide an example of how intensity measurements could be useful for distinguishing between several possible stacking sequences.

The detailed in-plane structures observed in the alkali metal compounds for stages  $n \geq 2$  are more complicated than would be implied by the simple geometric arguments based on metallic in-plane densities given in Table 1. For example, stage 2 compounds with K, Rb and Cs, all exhibit several phase transitions, the most important of which are common to the three compounds and are characterized by the transition temperatures  $T_1$  and  $T_u$ . Good agreement is obtained for values of  $T_1$  and  $T_u$  as determined by transport [14], X-ray [6, 15 - 17] and electron diffraction [2, 3, present work]. These transition temperatures thus define three temperature regimes: (1)  $T < T_1$ , (2)  $T_1 < T < T_u$  and (3)  $T > T_u$ . In each temperature regime, characteristic electron diffraction patterns are observed. For  $T < T_1$ , commensurate superlattice behavior dominates, in contrast to the regime  $T_1 < T < T_u$  where incommensurate superlattice behavior is dominant. For  $T > T_u$ , *spot* diffraction patterns are observed for second stage K, Rb and Cs compounds, indicative of *coexisting ordered* phases. We emphasize the implication of *coexisting ordered* phases from electron diffraction results, in contrast with the disordered phases [15 - 17] and lattice gas phases [18] reported by other workers for  $T > T_u$  based on analysis of X-ray diffraction measurements. Despite differences in the interpretation of the results, it is useful to note that there is significant agreement in several aspects of the X-ray and electron diffraction data.

On the basis of a phase diagram developed by Berker *et al.* [3], the electron diffraction patterns observed for each of the three temperature regimes for stage 2 graphite-K have been identified. For  $T < T_1$ , the observed pattern is consistent with the coexistence of a  $p(\sqrt{3} \times \sqrt{3})$  phase with  $\alpha\beta\gamma$  stacking and a disordered phase. In some parts of the sample, a small amount of  $p(\sqrt{7} \times \sqrt{7})R19.1^\circ$  phase is also observed. For  $T_1 < T < T_u$ , a ring diffraction pattern (powder pattern) is observed and identified with small



islands of ordered intercalate, incommensurate and orientationally unlocked with respect to the graphite. It is further suggested that these islands are surrounded by disordered regions. The observed rings consist of one set that is somewhat dilated from a commensurate ( $\sqrt{3} \times \sqrt{3}$ ) superlattice and a second set that is somewhat contracted from a commensurate ( $\sqrt{7} \times \sqrt{7}$ ) superlattice. The diameters for the most intense rings correspond to  $\vec{q}$  vectors that are in good agreement with  $\vec{q}$  vectors observed for the X-ray diffraction peaks for stage 2 graphite-potassium. Above  $T_u$ , distinct spot patterns are found superimposed on the rings. These unique patterns are interpreted in terms of islands orientationally locked to the graphite (spot patterns) surrounded by smaller islands that remain unlocked (ring patterns), in addition to disordered regions. The superposition of the spot and ring patterns implies that the dimensions of the intercalate lattice vectors are the same in the orientationally locked and unlocked islands.

A remarkable change in the real space image occurs as  $T$  passes through  $T_u$ . Below  $T_u$ , the real space image exhibits a profusion of small, randomly-distributed dark regions identified with the dense (as determined by X-ray fluorescence measurements) ordered islands, in addition to small light regions identified with the dilute ordered islands, superimposed on a gray background with intercalate concentration intermediate between that of the two types of islands. Above  $T_u$  the islands coalesce to form distended, dark and light structures, identified with the orientationally locked regions. Some of the small, light and dark structures remain, and these are identified as the unlocked islands. A mechanism has been proposed which simultaneously explains island coalescence and orientational locking [3]. The observation of dark and light islands in the real space images, and their identification, by X-ray fluorescence measurements, with the more dense and less dense intercalate regions, supports the identification of the electron diffraction pattern with coexisting phases. The reversibility of the electron diffraction pattern, and of the size distribution of the real space images, as the temperature is cycled across  $T_u$  indicates that the electron beam causes no appreciable radiation damage or epitaxial surface growth for temperatures  $T < T_u$  and  $T \sim T_u$ .

A dramatic change in the real space images is also observed at  $T_u$  for stage 2 graphite-Rb [2]. For the Rb intercalant, some parts of the sample exhibit commensurate  $p(\sqrt{7} \times \sqrt{7})R19.1^\circ$  regions for  $T_1 < T < T_u$ , and other parts exhibit a ring pattern indicative of incommensurate islands unlocked from the graphite. The measured  $\vec{q}$ -vectors for each ring observed with the Rb intercalant are given in Table 3 and compared with the corresponding  $\vec{q}$  vectors for the potassium intercalant and with  $\vec{q}$  vectors reported by Suematsu *et al.* [18] on the basis of neutron diffraction measurements on stage 2 graphite-Rb. It is significant that similar  $\vec{q}$  vectors are found for the ring patterns for the Rb and K intercalants. Since X-ray (00 $l$ ) intensity measurements on similarly prepared stage 2 samples with K and Rb indicate different in-plane densities for Rb and K [10], the similarity of the measured ring diameters provides further support for the presence of coexisting phases, with relative concentrations appropriate to yield the proper in-plane densities.

TABLE 3

Measured  $\vec{q}$  ve  
 $T_1 < T < T_u$

Electron diffra  
 $\vec{q}$  vectors in ( $\text{\AA}^{-1}$ )  
stage 2 graphit

1.24  
1.47  
1.79  
2.13  
2.52  
2.94  
3.20  
3.70

\*After Suematsu

Below  $T_u$  profusion of raised above regions, similar the diffraction real space, the is cycled across real space image should also be mine the electron the real space responding to imaging technique (diameter) of the nation of the dark field image stage  $n \geq 2$  co tion at  $T_u$  further calation comparison samples used in diffraction study diffraction wh diagrams.

Acknowledgments

We gratefully and useful discussions carrying out the



TABLE 3

Measured  $\vec{q}$  vectors for stage 2 compounds with intercalants K and Rb for  $T_l < T < T_u$

Electron diffraction $q$ vectors in ( $\text{\AA}^{-1}$ ) stage 2 graphite-Rb	Neutron diffraction* $q$ vectors in ( $\text{\AA}^{-1}$ ) stage 2 graphite-Rb	Electron diffraction $q$ vectors in ( $\text{\AA}^{-1}$ ) stage 2 graphite-K
1.24	1.20	1.28
1.47	—	—
1.79	1.78	1.78
2.13	2.08	2.18
2.52	2.40	2.61
2.94	2.95	2.96
3.20	—	3.29
3.70	—	3.71

\*After Suematsu *et al.* [18].

Below  $T_u$  the real space image for the stage 2 graphite-Rb exhibits a profusion of randomly distributed small islands as shown in Fig. 5. As  $T$  is raised above  $T_u$ , the islands coalesce to form larger, distended, dark and light regions, similar to the behavior observed for stage 2 graphite-K. For both the diffraction pattern in reciprocal space and the electron micrographs in real space, the observed changes in pattern are reversible as the temperature is cycled across  $T_u$ . The striking change in the island size and shape of the real space images at  $T_u$  is significant for both the K and Rb compounds. It should also be noted that in the electron microscope it is possible to determine the electron diffraction pattern corresponding to a particular region in the real space image, and *vice versa* to examine the real space image corresponding to specific diffraction spots. In application of the real space imaging techniques, bright field images are used to select regions ( $\sim 1 \mu\text{m}$  diameter) of the sample where electron diffraction patterns are taken. Examination of the real space origin of a given diffraction spot involves use of the dark field imaging technique. The observation of island formation in the stage  $n \geq 2$  compounds and the dramatic change in island size and distribution at  $T_u$  further support the presence of coexisting phases in these intercalation compounds. Possible differences in in-plane densities between samples used in the electron microscopy studies [1 - 3] and in the X-ray diffraction studies [14 - 17] would yield results for electron and X-ray diffraction which pertain to different paths on density-temperature phase diagrams.

### Acknowledgments

We gratefully acknowledge Dr Harry Mazurek for technical assistance and useful discussions, and the support of NSF-DMR Grant #78-10858 in carrying out this research.

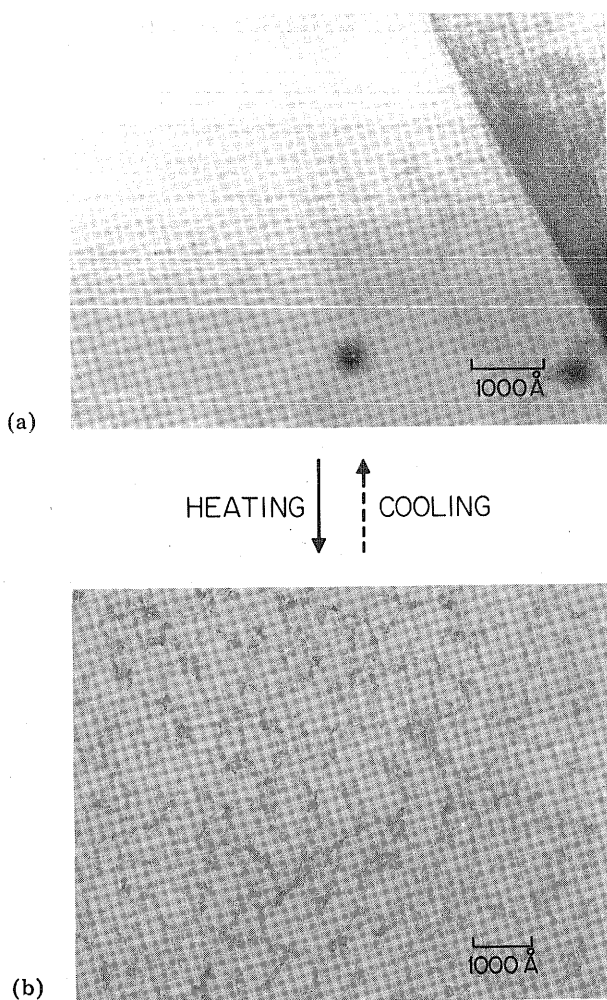


Fig. 5. (a) Bright-field image for a stage-2 graphite-Rb compound taken at 110 K. This micrograph is typical of low temperature electron micrographs taken below  $T_u$ . The dark areas are identified with islands ( $\sim 40$  Å dia.) of higher intercalate density than the lighter background. (b) Bright-field image taken on the same spot of the sample as in (a) but at  $T = 223$  K. Large islands ( $\sim 180$  Å in dia.), and coalescence and channeling of islands are typical of micrographs taken above  $T_u$ . A reversible change between the patterns (a) and (b) is found on heating and cooling of the sample across  $T_u$ .

## References

- 1 N. Kambe, M. S. Dresselhaus, G. Dresselhaus, S. Basu, A. R. McGhie and J. E. Fischer, *Mater. Sci. Eng.*, **40** (1979) 1.
- 2 N. Kambe, G. Dresselhaus and M. S. Dresselhaus, *Phys. Rev. B*, **21** (1980) 3491.
- 3 A. N. Berker, N. Kambe, G. Dresselhaus and M. S. Dresselhaus, submitted for publication.

- 4 G. S. Parry, *istry, Lond*
- 5 P. Lagrange
- 6 G. S. Parry, Nixon, K. I.
- 7 D. Guérard
- 8 W. Rüdorff
- 9 R. W. G. W
- 10 S. Y. Leung, *haus, Solid*
- 11 G. S. Parry,
- 12 A. Hérol, *tures, Vol.*
- 13 N. Wada, R
- 14 J. B. Hastin
- 15 H. Zabel, S
- 16 R. Clarke, I
- 17 N. Caswell,
- 18 H. Suemats

- 4 G. S. Parry, *Third Conf. Industrial Carbon and Graphite*, Society of Industrial Chemistry, London, 1971, p. 58.
- 5 P. Lagrange, M. El Makrini, D. Guérard and A. Hérold, *Physica*, 99B (1980) 473.
- 6 G. S. Parry and D. E. Nixon, *Nature (London)*, 216 (1967) 909; G. S. Parry, D. E. Nixon, K. M. Lester and B. C. Levene, *J. Phys. C*, 2 (1969) 2156.
- 7 D. Guérard and A. Hérold, *Carbon*, 13 (1975) 337.
- 8 W. Rüdorff and E. Schulze, *Z. Anorg. Allg. Chem.*, 277 (1954) 156.
- 9 R. W. G. Wyckoff, *Crystal Structures*, Vol. 1, Interscience, New York, 1964.
- 10 S. Y. Leung, C. Underhill, G. Dresselhaus, T. Krapchev, R. Ogilvie and M. S. Dresselhaus, *Solid State Commun.*, 32 (1979) 635.
- 11 G. S. Parry, *Mater. Sci. Eng.*, 31 (1977) 99.
- 12 A. Hérold, in F. Lévy (ed.), *Physics and Chemistry of Materials with Layered Structures*, Vol. 6, Reidel, Dordrecht, 1979, p. 323.
- 13 N. Wada, R. Clarke and S. A. Solin, *Synth. Met.*, 2 (1980) 27.
- 14 J. B. Hastings, W. D. Ellenson and J. E. Fischer, *Phys. Rev. Lett.*, 42 (1979) 1552.
- 15 H. Zabel, S. C. Moss, N. Caswell and S. A. Solin, *Phys. Rev. Lett.*, 43 (1979) 2022.
- 16 R. Clarke, N. Caswell, S. A. Solin and P. M. Horn, *Phys. Rev. Lett.*, 43 (1979) 2018.
- 17 N. Caswell, S. A. Solin, T. M. Hayes and S. J. Hunter, *Physica*, 99B (1980) 463.
- 18 H. Suematsu, M. Suzuki, H. Ikeda and Y. Endoh, *Synth. Met.*, 2 (1980) 133.

at 110 K. This  
low  $T_u$ . The dark  
y than the lighter  
as in (a) but at  
ng of islands are  
patterns (a) and

and J. E. Fischer,

.980) 3491.  
itted for publica-